



HAL
open science

Ultrasonic measurements with embedded Fiber Bragg Gratings in polyurethane resins

Nicolas Derrien, Maximilien Lehujeur, Xavier Chapeleau, Béatrice Yven, Guillaume Laffont, Nicolas Roussel, Thomas Blanchet, Arnaud Recoquillay, Olivier Durand, Gautier Gugole, et al.

► To cite this version:

Nicolas Derrien, Maximilien Lehujeur, Xavier Chapeleau, Béatrice Yven, Guillaume Laffont, et al.. Ultrasonic measurements with embedded Fiber Bragg Gratings in polyurethane resins. 11th European Workshop on Structural Health Monitoring - EWSHM 2024, DGZfP, Jun 2024, Potsdam, Germany. 10.58286/29636 . hal-04943131

HAL Id: hal-04943131

<https://univ-eiffel.hal.science/hal-04943131v1>

Submitted on 14 Feb 2025

HAL is a multi-disciplinary open access archive for the deposit and dissemination of scientific research documents, whether they are published or not. The documents may come from teaching and research institutions in France or abroad, or from public or private research centers.

L'archive ouverte pluridisciplinaire **HAL**, est destinée au dépôt et à la diffusion de documents scientifiques de niveau recherche, publiés ou non, émanant des établissements d'enseignement et de recherche français ou étrangers, des laboratoires publics ou privés.



Distributed under a Creative Commons Attribution 4.0 International License

Ultrasonic measurements with embedded Fiber Bragg Gratings in polyurethane resins

Nicolas DERRIEN¹, Maximilien LEHUJEUR¹, Xavier CHAPELEAU², Béatrice YVEN³, Guillaume LAFFONT⁴, Nicolas ROUSSEL⁴, Thomas BLANCHET⁴, Arnaud RECOQUILLAY⁴, Olivier DURAND¹, Gautier GUGOLE¹, Sébastien PRAMPART⁵, Robin NAYLOR⁵ and Odile ABRAHAM¹

¹ Université Gustave Eiffel, GéoEND, Bouguenais, F-44340, France

² Université Gustave Eiffel, COSYS-SII, I4S Team (Inria), F-44344, Bouguenais, France ³ ANDRA, 1/7 rue Jean Monnet, 92298 Châtenay-Malabry cedex, France

⁴ Université Paris-Saclay, CEA LIST, F-91120, Palaiseau, France

⁵ AFC-STAB Composite, St Hilaire de Chaléons, France

Abstract. In geophysics, Distributed Acoustic Sensing (DAS) optical fibers are increasingly being exploited to probe the subsurface using seismic waves. However, the integration of the deformation undergone by the fiber over a gauge length (typically a few meters) and a limited sampling frequency prohibit the use of this technology for ultrasonic applications. On the other hand, Fiber Bragg Gratings (FBG) offer a sufficiently small sensitive element (500 μm to several cm) to measure the dynamic deformation field at ultrasonic frequencies. Recently, it has been shown that FBGs bonded to a surface or embedded in a structure can be used to measure the dynamic deformation field caused by the propagation of an ultrasonic wave.

However, when inserting an optical fiber into a material, the effects of the structure on the fiber mechanical and optical properties need to be taken into account. For FBGs embedded in a reacting material, such as a polymer or concrete, the transient hardening stage can affect the FBG spectrum leading to a variation of the Bragg wavelength, a decrease of the grating amplitude and, in the worst case, a modification of the FBG signature (lobe broadening, introduction of harmonics, etc.) due to the strain induced by the material in the fiber.

In order to prepare for large-scale on-site measurements with embedded FBGs, it is necessary to carry out preliminary laboratory tests to address the instrumentation issues associated with inserting optical fibers into a curing material. For this purpose, several FBGs with different characteristics (insensitive to bending, acrylate/polyimide coating, multi-core, etc.) have been integrated into different polyurethane resins to compare their response to insertion, heat transfer and the measurement of dynamic deformations at ultrasonic frequencies. In this contribution, the reduced scale models produced in polyurethane resins and the results related to fiber insertion and ultrasound measurements are presented.

Keywords: Ultrasound · Fiber Bragg Gratings · Physical reduced scale modeling.



Introduction

Since their emergence in the 70's, the Optical Fiber (OF) technology has revolutionized the way information is exchanged by providing a method of transfer that travels at the speed of light. This period marked a turning point in telecommunications, but also allowed the emergence of new sensors. Nowadays, due to their several advantages, optical fibers are used as sensors in many fields, including civil engineering, geophysics and medicine to measure parameters like strain or temperature.

The Fiber Bragg Grating (FBG) is an optical fiber sensor introduced at the end of the 70's (Hill et al., 1978). It was initially used as a static deformation or temperature sensor. Betz et al. (2003) first demonstrated the possibility of using this technology to measure a dynamic strain field associated with the propagation of an ultrasonic wave using the *edge filtering* method (Melle et al., 1992). It was firstly employed to measure Lamb wave signatures propagating on the surface of a metallic plate using a bonded FBG. Later, Takeda et al. (2005) used this non-intrusive sensor to measure different Lamb wave modes with a Bragg grating buried between two layers of Carbon Fiber Reinforced Polymer (CFRP) laminate. More recently, Recoquillay et al. (2020) have demonstrated the possibility of using FBGs with passive techniques, that is acquiring ambient noise without any supplementary actuator, to image a defect located at the surface of a plate.

The number and the type of mechanical protecting layers added around the fiber core has a non-negligible impact on the strain transferred to the FBG sensors. Indeed, the greater the number of layers, the less deformation is transmitted to the fiber core (Zhou et al., 2006). In addition, the rate of deformation transmitted to the fiber core varies according to the material of the fiber coating (Chapeleau et al., 2021). Thus, reducing the number of layers around the FBG is expected to improve the sensitivity of this sensor to a strain field.

However, inserting a FBG without additional external protecting layers into a structure, exposes it to potentially strong internal shrinkage, bending or heat variations, which may modify the reflected optical spectrum (amplitude and central wavelength of the reflectivity peak) or potentially damage the FBG.

In this study, we show ultrasonic measurements carried out with FBGs embedded in polyurethane resins. We first compare the relative variations of the reflectivity peak of FBGs inscribed on five different types of OFs embedded in two polyurethane resins before and after their curing process. We then compare the amplitude of ultrasonic signals measured by the different types of embedded OFs using the *edge filtering* method.

1. Materials and Methods

1.1 Instrumentation of the resin samples

In order to compare the influence of the material, two cylindrical samples in polyurethane resin were instrumented with OFs embedded along the longitudinal axis of the sample (Fig. 1a). The first sample was made of pure Sika Biresin[®] F50 hereafter denoted as F50P. The second sample was made of the same resin loaded with 24% by mass of glass micro-beads (RZ1476), which we denote as F50B24. Loading polyurethane resins with additional charges is commonly used to modify the mechanical properties of the resin, to mitigate the shrinkage and exothermal reactions taking place during the curing process (polymerization). Each sample was casted in a mold with the OFs previously installed (Fig. 1a). The geometry chosen for these samples is a cylinder 200 mm long and 30 mm in diameter (Fig. 1b and 1c).

The optical fibers were disposed on a 10 mm diameter circle centered around the axis of the cylinder and 3 FBGs were inscribed on each of them at a Bragg wavelength of 1540, 1550 and 1560 nm respectively. The FBGs of each fiber are respectively located at 50, 100

and 150 mm from the end of the sample (Fig. 1c). Two of the etched fibers are standard Telecom SMF-28 fibers, one coated with acrylate (fiber A in Table 1) with a diameter of 245 μm , and the other with polyimide (fiber P in Table 1) with a diameter of 125 μm . Two other fibers, coated with polyimide, are insensitive to bending (BIF125 and BIF80 in Table 1). The last fiber has 7 cores (7C in Table 1), arranged in a hexagon with one core in the center, all in a 245 μm acrylate coating. Each core is a single-mode fiber 125 μm in diameter, but only the central core is etched in this study. It is possible to add protective layers to these fibers, but we have chosen to keep the protective layer to a minimum in order to quantify the effect of resin polymerization on FBGs.

Table 1. Name and specifications of optical fibers embedded in the two samples F50P and F50B24. The coating diameter indicates the total diameter of the fibers.

Fiber name	Fiber type	Cladding diameter	Coating diameter	Coating type
A	Standard Telecom Single Mode Fiber (SMF-28)	125 μm	245 μm	Acrylate
P	Standard Telecom Single Mode Fiber (SMF-28)	125 μm	155 μm	Polyimide
BIF125	Bend-Insensitive fiber (BIF), single mode	125 μm	154 μm	Polyimide
BIF80	Bend-Insensitive fiber (BIF), single mode	80 μm	100 μm	Polyimide
7C	7 cores fiber, single mode	125 μm	245 μm	Acrylate

1.2 Measurement of the static FBG spectra

To determine the static variations endured by the FBGs during the casting and curing processes, we analyzed the reflectivity spectra of the Bragg gratings before the casting and after the curing process using a Bragg meter connected to a computer (Fig. 2). A pulse light from 1530 to 1570 nm was sent into the core of the fibers and the reflected spectra were recorded showing the reflectivity of the three FBGs near wavelengths 1540, 1550, 1560 nm for FBGs 1, 2 and 3 respectively. This method allows us to quantify the shift of the central wavelength of the FBGs and the variations of the amplitude and the shape of the reflected spectrum for each Bragg.

1.3 Ultrasound measurement chain

The system used to perform dynamic strain measurements was different from the one presented above. It was composed of an “optical part” developed by the CEA, based on the *edge filtering* technique and including the tunable laser sources, the embedded fibers and the photo-diodes dedicated to the conversion of the optical signal reflected from the FBGs into an analog electric signal. The other part was dedicated to the acquisition of the mechanical waves and is referred to as the “mechanical part”, including the ultrasonic source, the analog filter and the acquisition system of the dynamic strain signal.

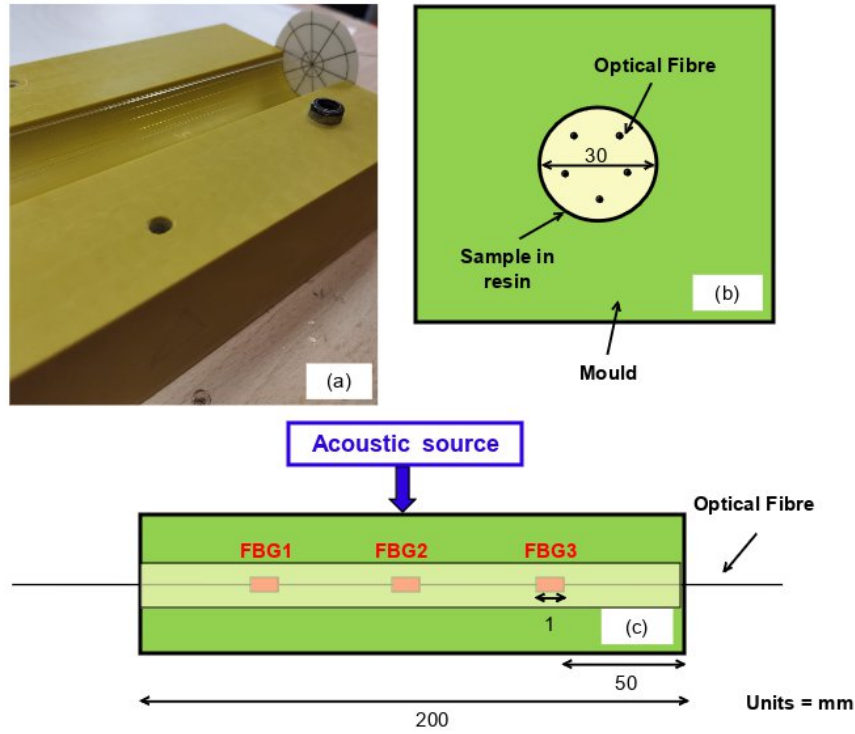


Fig. 1. Molds instrumented with optical fibers and schemes showing the geometry of the samples. (a) Photograph of an open mold before casting, with the optical fibers positioned. (b) Front view of the mold and resin sample. (c) Schematic longitudinal section of the mold showing the positioning of the FBGs along each fiber. FBG1, FBG2 and FBG3 denote the three Bragg gratings for one fiber.

1.3.1 FBG spectrum acquisition: calibration of the setting point for the edge filtering method

In this work, the optical system was configured to interrogate two FBGs simultaneously (on two separate fibers).

Prior to acoustic measurements, the reflectivity peak of each FBG was measured and displayed in order to tune the wavelength of the laser source on the nearly linear edge of the FBG reflectivity peak, as required by the *edge filtering* method.

For each FBG, we used a tunable optical source (Fig. 3a) capable of emitting a laser between wavelengths 1527 and 1621 nm. The intensity of the laser source was controlled using optical attenuators (see Fig. 3b). An optical circulator (Fig. 3c) was used to connect the laser source to the optical fiber to be interrogated (Fig. 3d) and to transmit the light reflected back from the Bragg grating to a photo-diode (Fig. 3e). The obtained analog signal was sampled at a low acquisition rate using a *National Instrument* acquisition card (see Fig. 3f) connected to the computer to display the FBG spectra and to control the laser sources (see Fig. 3g). Once the Bragg spectrum is displayed, the wavelength of the laser source is set on the edge of the FBG spectrum to use the *edge filtering* method.

1.3.2 Ultrasonic wave acquisition using FBG

The analog signals from the photo-diodes, were bandpass filtered between 30 and 250 kHz (Fig. 4b) and recorded using an oscilloscope (Fig. 4c).

The acoustic source signal was a door function of length 5 μ s emitted by the generator (Fig. 4c) and sent to an acoustic source Olympus V1011, resulting in a pulse centered at about 100 kHz. A conceptual scheme of the acoustic measurement set up is presented on Fig. 4e. The acoustic source was placed on top of the mold including the resin sample and the deformation caused by the mechanical wave was recorded by the desired FBG.

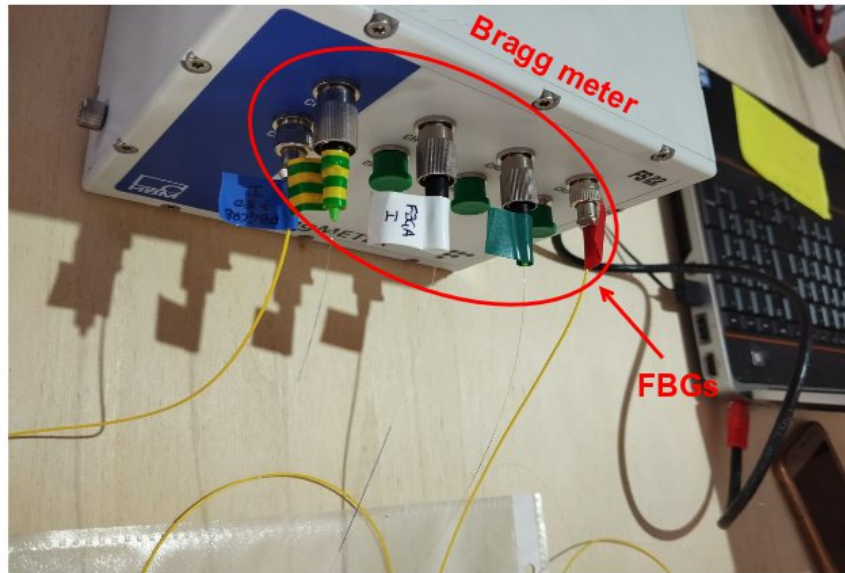


Fig. 2. Equipments used to measure the FBG spectra. A view of the connecting part between the FBGs and the Bragg-meter.

2. Results

2.1 Comparison of the effect of the curing process of two polyurethane resins on the amplitude of the reflectivity peak of FBGs inscribed on the different types of optical fibers

Using the Bragg-meter, we measured the Bragg reflectivity spectra before the casting and after the curing process of the resins for each OF type and each sample.

The static shifts in wavelength of the FBGs reflectivity peaks (not shown) indicate that the F50B24 sample encountered much lower shrinkage than F50P, which we interpret as the result of the load added in the F50B24 sample.

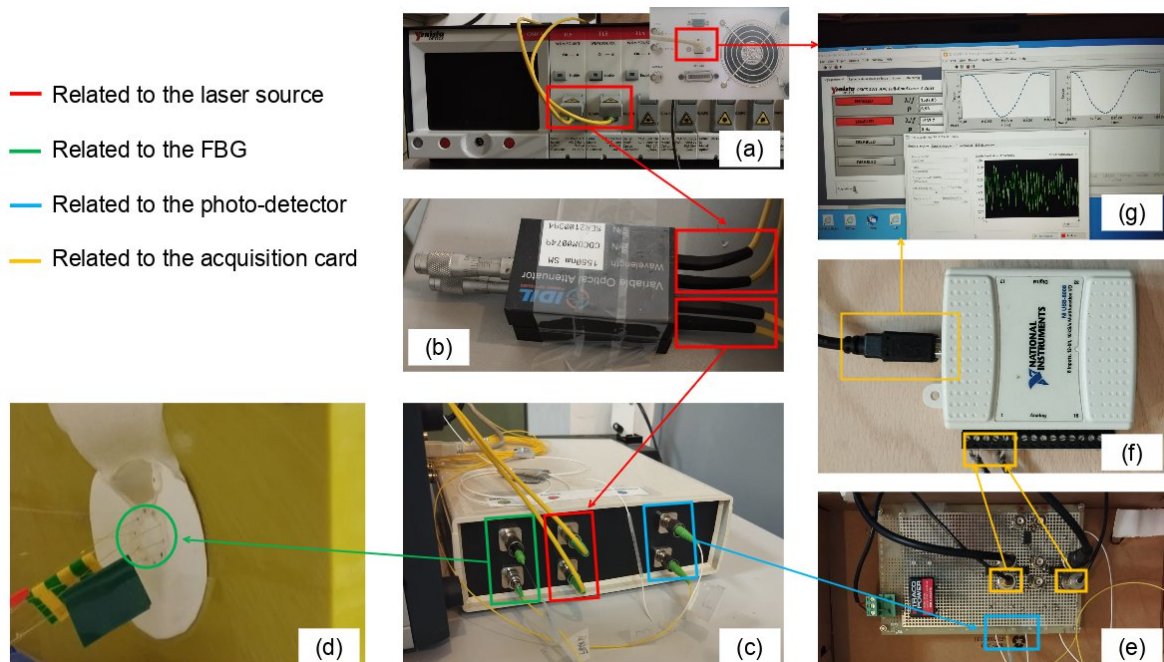


Fig. 3. “Optical part” of the measurement chain. It includes (a) the two optical sources, (b) two optical attenuators, (c) the circulator, (d) the optical fibers embedded into a resin sample (F50P or F50B24), (e) the photodiode card connected to (f) the acquisition card used to monitor the FBG reflectivity at a low acquisition rate and to control the laser source and (g) the computer and graphical interface.

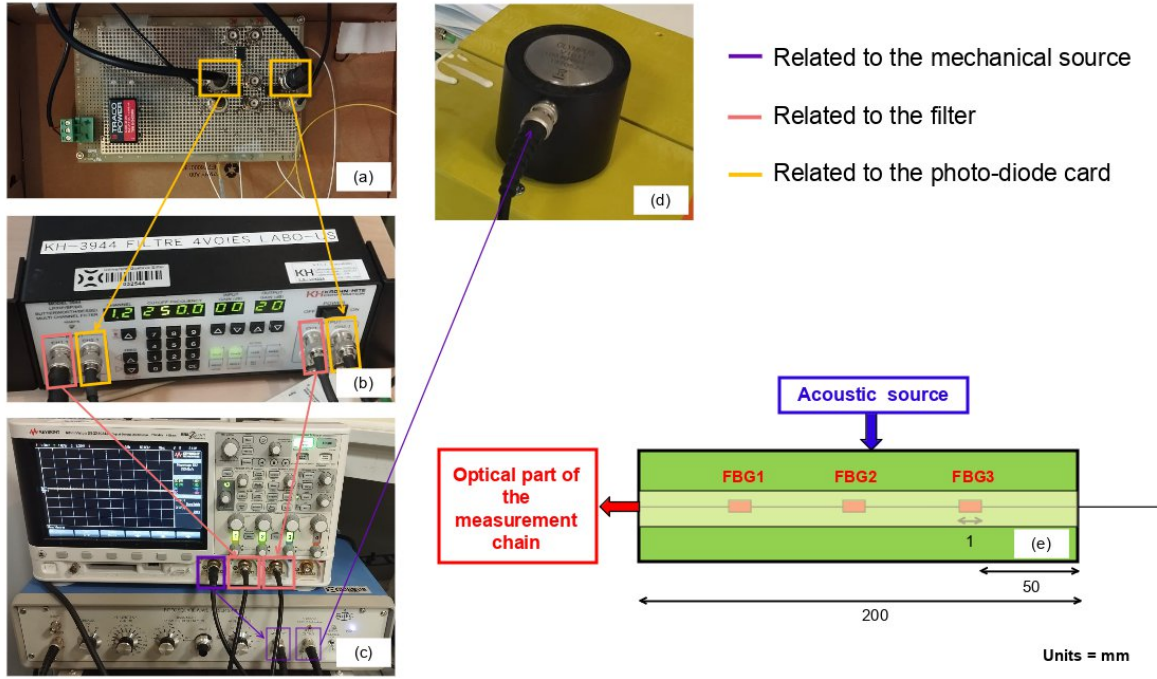


Fig. 4. “Mechanical part” of the measurement chain. (a) Photo-diode card, (b) analog acoustic filter, (c) oscilloscope and source generator, (d) acoustic source disposed on top of the mold including the resin sample and, (e) conceptual scheme of the measurement system showing the positioning of the acoustic source. FBG1, FBG2 and FBG3 denote the 3 Bragg gratings of each optical fiber.

The relative variations ΔR of the maximum amplitudes of the reflectivity peaks for all the FBGs and samples are shown in Fig. 5. This relative variation is calculated as follows:

$$\Delta R = \frac{R_{aftercasting}^{max} - R_{beforecasting}^{max}}{R_{beforecasting}^{max}} \times 100,$$

where $R_{after/beforecasting}^{max}$ corresponds to the maximum amplitude of the reflectivity peak of the FBG before or after casting.

For the F50B24 sample, characterized by lower shrinkage, we observed weaker variations in the relative amplitude of the reflectivity peaks for all the FBGs (Fig. 5a). For this sample the amplitude variations were comparable for all the fibers. The observed variations (-20 to +20%) appeared insignificant and possibly related to the connection between the FBGs and the Bragg-meter.

For the F50P sample (Fig. 5b) characterized by a stronger shrinkage, the amplitude of the reflectivity peaks of the FBGs inscribed on the BIF and 7C fibers (Table 1) remained relatively unaffected by the curing process. However, the reflectivity peaks from FBGs inscribed in P and A fibers (Table 1) were undetectable for 5 out of 6 FBGs. Indeed, after the curing process of the F50P, the FBGs inscribed on the BIF125 and BIF80 showed a maximum loss of 20% of their reflectivity peak compared to 100% for the FBGs inscribed in the P fiber. As a result, the FBGs inscribed in the P and A fibers in the F50P samples could not be used for ultrasonic measurements.

This significant difference suggests that the BIF and 7C fibers are more suited than standard Telecom fibers for materials with strong shrinkage. But it is important to notice that these variations are relative and that they only represent the effect of the material shrinkage on the FBGs reflectivity peak before and after casting, and not the absolute reflectivity values. For the 7C fiber embedded in the F50P sample, the absolute reflectivity peak was much lower than for F50B24 (not shown).

For the A fiber in the F50P sample, the variations of the reflectivity peaks depend on the position of the FBG (FBG1, 2 or 3, Fig. 5b). Indeed, we observed that the reflectivity

peak of FBG1 was not affected by the curing process of the F50P resin. However, the two other FBGs show a variation of their reflectivity peaks that is more coherent with the variation found for the P fiber (between 80 and 100 % of reflectivity loss). The reason why the FBG1 of the A fiber better resisted to the curing process of the F50P than FBG2 and FBG3 is still unclear at this stage.

2.2 Ultrasonic measurements with FBGs embedded in materials with shrinkage

Two series of ultrasonic measurements obtained with the experimental set up described in section 1.3.2 are shown in Fig. 6 for the Bragg grating FBG2 (located in the center of the samples, Fig. 4e) of each OF and for the two samples F50B24 (Fig. 6a) and F50P (Fig. 6b). These measurements confirmed that all the FBG2s embedded in the F50B24 were available for ultrasonic measurements. Nevertheless, the signals were different in terms of amplitude and waveform even within the same sample. The position of the acoustic source and the spatial distribution of the FBG2 relative to the source may explain these differences.

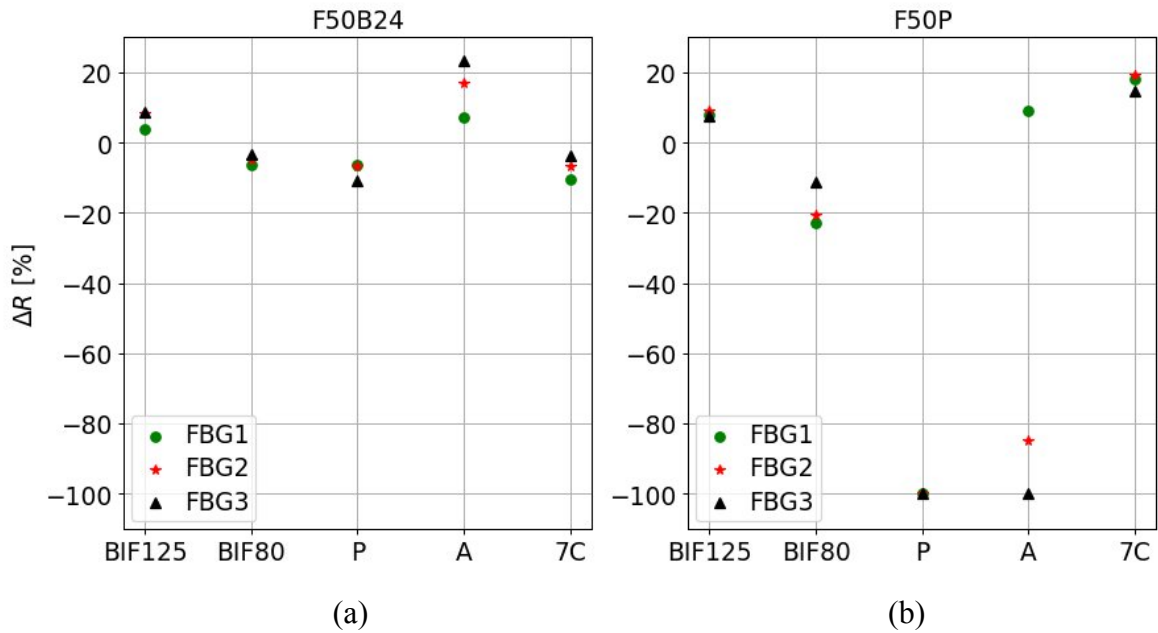


Fig. 5. Relative variations of the reflectivity peak of the 3 FBGs of each OF type before the casting and after the curing process for the (a) F50B24 and (b) F50P samples. The names on the abscissa refer to the name of the fibers in Table 1. The notations FBG1, FBG2 and FBG3 represent the 3 FBGs of one OF.

Indeed, the acoustic source was located on top of the mold almost directly above the position of FBG2 for all the fibers, but the circular distribution of the OFs inside the sample implies that the FBGs are not at the same distance from the acoustic source. The first-arrival times also follow this reasoning, since we observe that for both resins they oscillate around 19 μ s, but are not exactly the same from one FBG to another.

For the F50P sample, no signal could be acquired for the FBG2 of the P fiber. This is explained by the total loss of the reflectivity peak for every FBGs inscribed in this fiber, as shown on Fig. 5b. In contrast, we could measure an ultrasonic signal with the FBG2 of the two BIF and also with the one inscribed in the A fiber despite the fact that this FBG had lost almost 85% of its reflectivity peak (Fig. 5b). Nevertheless, we note that the amplitude of the signal measured by the FBG2 of the 7C fiber is strongly attenuated compared to the others.

However, Fig. 6 confirms that we are able to measure an ultrasonic strain field with almost every FBGs embedded in a material undergoing shrinkage except for the FBGs inscribed on the P fiber which did not resist the shrinkage of the F50P resin.

4. Discussion

We have quantified the relative effect of the shrinkage of two polyurethane resins on the reflectivity spectrum of FBGs inscribed in different types of OFs. Then, we have demonstrated that in most cases, carrying out ultrasonic measurements with these buried sensors was possible. Nevertheless, some ways of improvement are still being investigated:

First, to quantify the effect of the material shrinkage on the reflectivity peak of the embedded FBGs, we observed that disconnecting and reconnecting the OF to the Bragg-meter may affect the absolute amplitudes of the reflected Bragg spectra, making them difficult to compare. So an improvement could be to quantify the uncertainty linked to the connexion between the FBGs and the Bragg-meter.

Second, for the ultrasonic measurements with embedded FBGs, the acoustic source was placed above the molds (Fig. 1) i.e. not directly in contact with the resin sample, and perpendicular to the axis of the optical fibers. As this sensor is known to be an unidirectional sensor with a radiation diagram showing a maximum of sensitivity for a strain field aligned with the axis of the OF, we expect that placing the source on one of the ends of the sample and coupling it with the resin sample could improve our ability to interpret the measured waves.

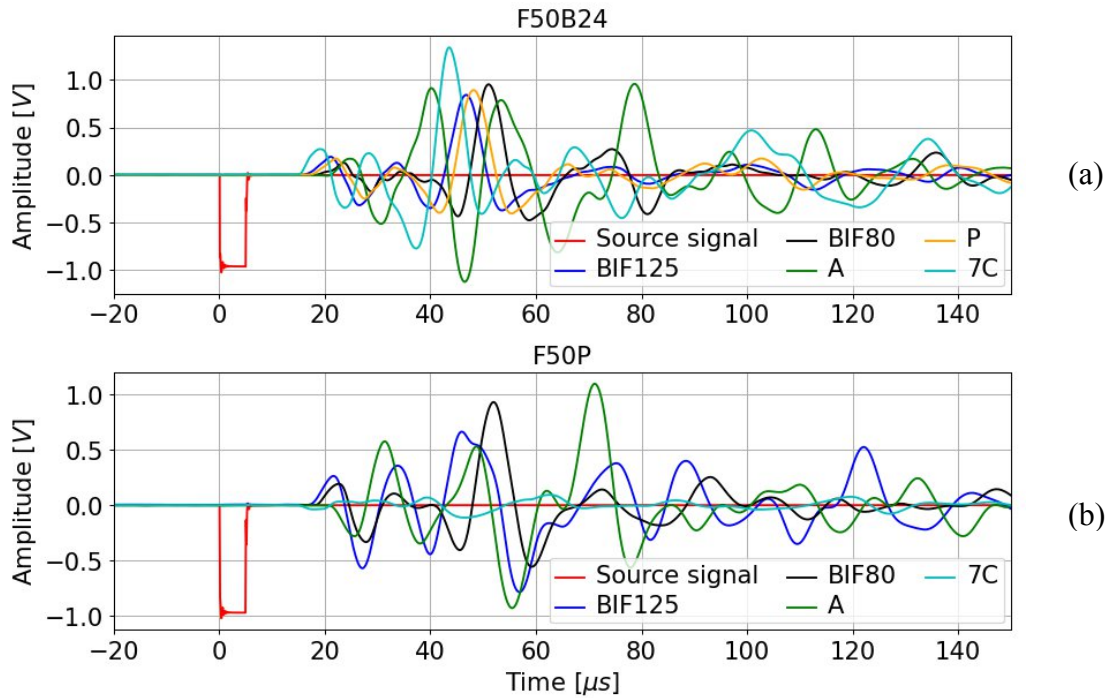


Fig. 6. Comparison of the dynamic strain signals measured by the FBG2 of the OF embedded in (a) the F50B24 sample (lower shrinkage) and (b) F50P (higher shrinkage). The displayed amplitudes correspond to the voltage measured at the output of the analog filter (Fig. 4b) and can be compared with each other.

5. Conclusion

This study showed the feasibility of performing ultrasonic measurements using embedded FBGs inscribed in 5 different types of optical fibers inside a casting polyurethane resin with and without additional micro-beads load. The challenge was to keep an usable sensor with minimum protecting layers when embedded into a material with shrink. For that, two BIFs, two SMF-28 fibers and one 7C fiber have been tested and compared in terms of amplitude losses of the FBGs reflectivity peaks induced by the material shrinkage. Moreover, we have carried out ultrasonic measurements with the same FBGs to know if it is pos-

sible to use them as dynamic strain sensors in that context. Our main results are listed hereafter:

First, the choice of the OF type must be constrained by the type of material into which we intend to insert it. In the case of the F50B24 resin, all types of OF could be exploited. On the contrary, in the case of the F50P resin, the A and P fibers showed significant variations in their reflectivity peaks.

Second, the BIF and the 7C fiber appeared to be a good solution to measure the dynamic strain with embedded FBGs into a material, where the internal shrinkage is problematic as shown by the experiment involving the F50P resin.

This study shows that the insertion phase of FBGs with as few protective layers as possible into a curing material depends mainly on the shrinkage regime applied to the OF. For a high shrinkage regime, the BIF seems to be the best solution, but for a lower shrinkage regime, the advantage of the BIF is negligible among the other type of OF tested. So a future work could be to test the influence of the coating on the ultrasound measurements for a material that does not affect too much the reflectivity peak of the FBGs like the F50B24.

Acknowledgment

Our research work is made possible by funding from the French ANR-21-CE04-0007 FO-US project.

References

- Hill, K. O., Fujii, Y., Johnson, D. C., and Kawasaki, B. S. (1978). Photosensitivity in optical fiber waveguides: Application to reflection filter fabrication. In: *Applied Physics Letters*. DOI: <https://doi.org/10.1063/1.89881>
- Betz, D. C., Thursby, G., Culshaw, B., and Staszewski, W. J. (2003). Acousto-ultrasonic sensing using fiber Bragg gratings. In: *Smart Materials and Structures*. DOI: <https://doi.org/10.1088/0964-1726/12/1/314>
- Melle, S. M., Liu, K., and Measures, R. M. (1992). A passive wavelength demodulation system for guided-wave Bragg grating sensors. In: *IEEE Photonics Technology Letters*. DOI: <https://doi.org/10.1109/68.136506>
- Takeda, N., Okabe, Y., Kuwahara, J., Kojima, S., and Ogisu, T. (2005). Development of smart composite structures with small-diameter fiber Bragg grating sensors for damage detection: Quantitative evaluation of delamination length in CFRP laminates using Lamb wave sensing. In: *Composites Science and Technology*. DOI: <https://doi.org/10.1016/j.compscitech.2005.07.014>
- Recoquilly, A., Druet, T., Nehr, S., Horpin, M., Mesnil, O., Chapuis, B., Laffont, G. and D'Almeida, O. (2020). Guided wave imaging of composite plates using passive acquisitions by fiber Bragg gratings. *The Journal of the Acoustical Society of America*. DOI: <https://doi.org/10.1121/10.0001300>
- Zhou, G., Li, H., Ren, L., and Li, D. (2006). Influencing parameters analysis of strain transfer in optic fiber Bragg grating sensors. In: *Advanced Sensor Technologies for Nondestructive Evaluation and Structural Health Monitoring II*. DOI: <https://doi.org/10.1117/12.661858>
- Chapeleau, X. and Bassil, A. (2021). A general solution to determine strain profile in the core of distributed fiber optic sensors under any arbitrary strain fields. In: *Sensors*. DOI: <https://doi.org/10.3390/s21165423>